University of Reading

β - sheet assembly in amyloidogenic glutamic acid nanostructures: insights from X-ray scattering and infrared nanospectroscopy

Article

Accepted Version

Mello, L. R., Hamley, I. W., Miranda, A., Alves, W. A. and Silva, E. R. (2019) β - sheet assembly in amyloidogenic glutamic acid nanostructures: insights from X-ray scattering and infrared nanospectroscopy. Journal of Peptide Science, 25 (6). e3170. ISSN 1099-1387 doi: https://doi.org/10.1002/psc.3170 Available at https://centaur.reading.ac.uk/83853/

It is advisable to refer to the publisher's version if you intend to cite from the work. See Guidance on citing.

To link to this article DOI: http://dx.doi.org/10.1002/psc.3170

Publisher: European Peptide Society and John Wiley & Sons

All outputs in CentAUR are protected by Intellectual Property Rights law, including copyright law. Copyright and IPR is retained by the creators or other copyright holders. Terms and conditions for use of this material are defined in the End User Agreement.

www.reading.ac.uk/centaur

University of Reading

CentAUR

Central Archive at the University of Reading

Reading's research outputs online

β-sheet Assembly in Amyloidogenic Glutamic Acid Nanostructures: Insights from X-ray Scattering and Infrared Nanospectroscopy

Lucas R. Mello[a], Ian W. Hamley[b], Antonio Miranda[a], Wendel A. Alves[c] and Emerson R. Silva[a*]

[a]Departamento de Biofísica, Universidade Federal de São Paulo, 04044-020, São Paulo, Brazil; [b]Department of Chemistry, University of Reading, RG6 6AD, Reading, UK; [c]Centro de Ciências Naturais e Humanas, Universidade Federal do ABC, 09210-580, Santo André, Brazil.

ABSTRACT

Glutamic acid-rich peptides are crucial to a variety of biological processes, including glutamatergic neurotransmission and immunological defense. Glutamic acid sequences often exhibit unusual organization into β_2-type sheets, where bifurcated *H*-bonds formed between glutamic acid side-chains and NH in amide bonds on adjacent β–strands play a paramount role for stabilizing the molecular assembly. Herein, we investigate the self-assembly and supramolecular structure of simplified models consisting of alternating glutamic acid/phenylalanine residues. Small-angle X-ray scattering and atomic force microscopy show that the aggregation pathway is characterized by the formation of small oligomers, followed by coalescence into nanofibrils and nanotapes. Amyloidogenic features are further demonstrated through fiber X-ray diffraction, which reveal molecular packing according to cross-β patterns, where β–strands appear perpendicularly-oriented to the long axis of nanofibrils and nanotapes. Nanoscale infrared spectroscopy from individual nanoparticles on dried samples shows a remarkable decrease of β_2-sheet content, accompanied by growth of standard β-sheet fractions, indicating a β_2-to-β_1 transition as a consequence of the release of solvent from the interstices of peptide assemblies. Our findings highlight the key role played by water molecules in mediating H-bond formation in β_2-sheets commonly found in amyloidogenic glutamic acid-rich aggregates

Key-words: peptide self-assembly; AFM-IR; peptide materials; β-amyloid

*Corresponding author: er.silva@unifesp.br

INTRODUCTION

Self-assembling oligopeptides have been identified as promising candidates in the development of the next generation of biomaterials.[1-3] Since they are based on a limited number of building blocks, these systems reduce the complexity of intra- and inter- molecular interactions, providing interesting models for the investigation of biological phenomena closely related to protein aggregation.[4-7] Furthermore, rationally-designed sequences are easy to synthesize through standard solid-phase approaches and exhibit higher stability and lower cost in comparison with longer peptides, proteins and enzymes.[2, 8] Obviously, this versatility attracts the interest of scientists from a broad range of disciplines, from chemistry and materials science to condensed matter physics and pharmacology. The ultimate goal of these efforts has been to discriminate the role of specific amino acids on the formation of oligomers appearing upon protein misfolding, which are often associated with degenerative diseases.[9, 10] Emblematic examples of this are amyloid structures formed by the so-called *Tjernberg* peptide,[11, 12, 13, 14] a pentameric fragment Aβ(16-20) of the amyloid beta (Aβ) peptide with composition K-L-V-F-F. Studies involving charged sequences have focused on cationic species,[15, 16, 17] most likely due to the extensive presence of these amino acids in bioactive segments such as cell-penetrating and antimicrobial peptides, neuropeptides, tumor-homing peptides and peptide hormones.[18] Their anionic counterparts, namely glutamic and aspartic acid-based sequences, are less studied, leading to a lack of information on this significant peptide class.[19]

In the current work, we present a detailed investigation on the self-assembly and structure of glutamic acid-based octapeptides with general sequence E-F-E-F-E-F-E-F (*E:* glutamic acid, *F:* phenylalanine). An ancillary issue arising from *N*-terminal glutamic acid (Glu) is the condensation of carboxylic side-chains and amino group into pyroglutamic acid upon loss of a water molecule[18, 20-22] and here we explore the co-assembly with species containing pyroglutamic acid at the N-terminus. In recent years, Glu-rich peptides have gained more attention mainly due to the ability of carboxylic side-chains to form certain types of H-bond networks.[23] Particularly, it has been demonstrated that Glu-enriched sequences stack into anti-

parallel sheets, forming β_2-type structures held together by bifurcated H-bonds between amide carbonyls and carboxylic acid side-chains in neighboring sheets.[24-27] These structural insights have been derived mainly from Fourier-transform infrared absorption (FTIR), circular and vibrational circular dichroism (CD and VCD).[24] The highly simplified sequence, containing only two different amino acid species, contains an *E* residue at the *N*-terminus. This feature mimics a class of peptide sequences found in nature, whose aggregation is yet to be explored in depth. For instance, a large fraction of recombinant antibodies possess an *N*-terminal Glu in light and heavy chains[20, 28, 29] and many compounds of biomedical interest, including T-lymphocyte vaccines,[30] have a Glu residue at the amide terminal. In addition, the link between amyloid oligomers and glutamatergic proteins has been the subject of intensive research in the last years.[31-34] The model peptides investigated here were carefully designed to take advantage of self-assembling properties exhibited by phenylalanine residues intercalated along the sequences. Particularly, benzene side chains enable aromatic interactions such as π–π stacking and ion-π interactions.[35,36] These features have been found to be crucial for directionality of self-assembly in amyloid aggregates, favoring growth of anisotropic arrays along a preferential axis, and giving raise to fibrils and tapes.[35] In addition, the presence of aromatic residues in amyloidogenic oligopeptides has been demonstrated to favor the formation of β–sheets, a keystone characteristic in the present study.

Herein, we explore both the self-assembly and the structure of glutamic acid-based peptides through different approaches by combining small-angle X-ray scattering (SAXS), fiber diffraction (fXRD) and atomic force infrared spectroscopy (AFM-IR). SAXS reveals multi-level self-assembly into polymorphs with internal structure built up throughout a hierarchical process, with aggregation ranging from fractal-like oligomers to fibrillar subunits associated into nanotapes and nanofibers. X-ray diffraction shows unequivocal amyloid-like features of the resulting self-assemblies, with the formation of cross-β structures, whereas AFM-IR reveals the spatial distribution of different types of β-structures with nanometer resolution.

METHODS

Peptide synthesis and sample preparation: The alternating glutamic acid/phenylalanine $[EF]_4$ peptide (E-F-E-F-E-F-E-F) was custom synthesized by Peptide Protein Research Ltd. (Fareham, UK). Synthesis was performed using solid phase methods, with Fmoc protected amino acids. Cleavage of the Fmoc group was carried out using piperidine, whilst cleavage from the resin and removal of the side chain protecting groups from the glutamic acid residues was achieved with TFA. The product was purified in acetonitrile and water containing 0.1 % NH_4OH prior to lyophilization. The ammonium salt form of N-terminal glutamic acid peptides is more prone to conversion into pyroglutamic acid upon cyclization between the N-terminus and the adjacent glutamic acid side chain.[20, 37] HPLC and electron spray mass spectrometry assessment showed the presence of populations with molar masses M_w = 1124.2 g/mol, corresponding to the $[EF]_4$ sequence, and M_w = 1106.1 g/mol, resulting from loss of a H_2O molecule upon conversion of the N-terminal glutamic acid residue into pyroglutamic acid (see SI file, Fig. S1). LC data obtained from solutions prepared in the same conditions used for the structural assays presented in this work (see below), indicated that the fraction of $[EF]_4$ was 68%, whereas the pyroglutamic-containing moiety - i.e., X-F-E-F-E-F-E-F (X = pyroglutamic acid residue, henceforth denoted $p[EF]_4$) – remained at 32%. Degradation tests such as heating of peptide solutions and exposure to environmental conditions, including contact with atmosphere and maintenance at room temperature for a period of weeks, did not increase the pyroglutamic fraction in the batches, suggesting that 68/32 is the equilibrium $[EF]_4$/$p[EF]_4$ ratio. No further impurities were identified by LC assays and the fraction of glutamic acid-rich octamers ($[EF]_4$ + $p[EF]_4$) was > 99%. Samples for SAXS and topography AFM assays were prepared using 20 mM NaOH (sodium hydroxide) in H_2O as a solvent. Samples for FTIR and Nano-IR experiments were prepared using 20 mM NaOD in D_2O (sodium deuteroxide) as a solvent. The peptide is not soluble in water at neutral pH due to the low pKa (= 4.1) of the glutamic acid side-chains.[19] To overcome this problem, sample preparation was carried out by dissolving the

peptide powder in 20 mM NaOH (or NaOD) solutions, adjusting to the desired concentrations. To assist solubilization, samples were heated to 60 °C and sonicated for 30 minutes immediately after dissolution. Samples at concentrations of 0.1 wt% and 1 wt% were in the form of transparent solutions. After this procedure, solutions were kept in the fridge (4 °C) before further assays and incubation times were about 24 hours prior to fluorescence experiments and about one week prior to SAXS, AFM and other spectroscopy assays. Highly-concentrated samples (i.e., 10 wt%) required longer sonication times to reach homogenization, typically a couple of hours, and transitioned to a gel state over the course of a few days in the fridge. Measurements indicated that solutions prepared at 0.1 wt% and 1 wt% had pH = 11.3 and 7.8, respectively. In the case of gelled samples (containing peptide at 10 wt%), pH was estimated at ~5 by using indicator paper.

Fourier-transform infrared Spectroscopy: FTIR spectroscopy was performed using a Nicolet Nexus spectrophotometer. Samples were prepared using D_2O as a solvent and NaOD to alkalize the medium. Droplets from a solution prepared at 1 wt% peptide were loaded between KBr windows, separated by 12 μm mica spacers. Spectra were recorded in the interval corresponding to the amide region, at a resolution of 4 cm^{-1}. Averages from 128 accumulations were background-subtracted and noise reduction was performed using FFT filters with smoothing windows of 6 data points.

Small-angle X-rays Scattering: Small-angle X-ray Scattering measurements were carried out on the SAXS-1 beamline at LNLS (Campinas, Brazil). For liquid samples, about 300 μl were loaded with a syringe into a 1 mm cell between mica windows. In the case of gels, a small amount of sample was sandwiched between Kapton films separated by a 0.5 mm path length. Ten frames, 30 s each, were grabbed per sample. The different frames were compared, in the absence of radiation damage, they were averaged, and background subtracted. The X-ray wavelength was λ = 1.54 Å and the sample-to-detector distance was 1000 mm leading to a q-range 0.12 $nm^{-1} \leq q \leq$ 4.5 nm^{-1}. Data were acquired using a Pilatus 1M detector and were

radially averaged with Fit2D using calibration parameters obtained from silver behenate patterns. Model fitting was carried by using the SASFit program.[38]

Fiber X-ray diffraction (fXRD): Oriented stalks were prepared by suspending droplets from a 10 wt% peptide solution placed between the ends of wax-coated capillaries. The capillaries were covered with Petri dishes, sealed with Parafilm and left to dry in the fridge for a few days. This procedure provided very slow drying and provided more oriented samples, leading to well-resolved XRD patterns. Stalks were vertically positioned in a RAXIS IV++X-ray diffractometer (Rigaku) endowed with a rotating anode generator and a Saturn 992 CCD camera (pixel size 89.8 μm²) was used to register the pattern. The sample-to-detector distance was fixed at 50 mm. Data reduction was carried out using Fit2D and unit-cell optimization was performed using the CLEARER software.[39]

Atomic Force Microscopy (AFM): AFM topography images were obtained on a Park NX10 instrument operating in tapping mode with tip frequencies of the order of 250 kHz. Droplets from peptide solutions were deposited onto freshly-cleaved mica substrates, left to rest for about 3-5 minutes and then rinsed with Milli-Q water. In the case of gel samples, dilutions with the corresponding NaOH solutions followed by vortexing steps were made just prior to casting onto mica surfaces. Scans across areas with 5 x 5 μm^2 or 1 x 1 μm² were performed to produce images with 512 x 512 pixels. Scan frequency was 0.5 Hz and relative humidity of the set up was kept below 3% using a flushing nitrogen stream prior to measurements. All measurements were carried out at room temperature. Data correction and analysis were performed with the software Gwyddion.

Nanoscale Infrared measurements (AFM-IR): Nanospectroscopy measurements were carried out on an Anasys NanoIR2-s microscope installed at the Laboratory for Surface Science of the Brazilian Nanotechnology National Laboratory (Campinas, SP). Samples were prepared by casting droplets from peptide solutions onto Au-coated silica substrates, letting them rest for a few minutes and then removing the excess of water with filter paper. The instrument operates in contact mode, using the thermal response of the sample to excite the resonance vibration of the cantilever.[40,41] Samples are illuminated by an infrared tunable laser whose electromagnetic field

is trapped between the Au-coated substrate and the AFM tip, forming a resonant nanocavity, which enhances signal-to-noise ratio. This set up allows measurements of IR absorption profiles as a function of the wavenumber, at spatial resolutions limited by the tip radius (~ 30 nm). In this case, the AFM tip was positioned on regions of interest corresponding to different nanostructures and infrared profiles were obtained in the range 1550 – 1800 cm^{-1}. All data were baseline subtracted (Au profile) and smoothed using an FFT filter (5 points of window). A second kind of experiment conducted on the NanoIR2-s microscope was the collection of "chemical images", using fixed wavenumber IR radiation and scanning the surface with the AFM tip. In such assays, *z*-axis expansion was observed as a consequence of thermal response due to local infrared absorption, and IR mapping of the surface could be obtained at nanoscopic resolution. The pulse repetition frequency of the laser - i.e., the frequency of the tip-substrate resonator - was typically around 250 kHz and images were collected in 5 × 5 μm^2 areas (512 × 512 pixels), with scanning speed of 1 line per second. Preliminary image treatment was performed using the AnalysisStudio software provided by Anasys and further visualization enhancement was carried out with the software Gwyddion.

RESULTS

X-ray Scattering and Fiber Diffraction Assays:

Preliminary assays using the pyrene fluorescence probe method[42] were carried out to determine the critical aggregation concentration (CAC) as reported elsewhere.[15, 43] These experiments are detailed in the SI file (Figure S2) and they indicated the appearance of aggregates in solution at a CAC ~ 0.1 wt%. Therefore, further experiments for structural characterization of nanoscopic aggregates were performed in samples at concentrations ≥ 0.1 wt%.

The *in-situ* nanostructure of the particles was probed using synchrotron SAXS. In Figure 1, SAXS data in the Porod representation (log-log plots) reveal that the structure depends

on concentration across the nanometer size scale. The small-angle region of scattering profiles from solutions containing lower peptide amounts (0.1 wt% and 1 wt% peptide) is characterized by a steep descent scaling with $q^{\sim -2.7}$, consistent with the presence of fractal aggregates.[44] On the other hand, the high-*q* range ($q > \sim 1.5$ nm^{-1}) features intensity decaying as $q^{\sim -1.6}$, suggesting that the local structure of aggregates comprises geometries between elongated and planar-like objects.[45] These two power-law regimes are separated by a plateau-like zone in the intermediate *q*-range. These features reveal that the data are complex, with multilevel structural information appearing in the profiles, and proper data fitting could not be carried by using standard shape models. In this case, to extract quantitative information, we performed model fitting adopting the unified exponential/power-law approach proposed by Beaucage,[46, 47] which is widely used to describe scattering from fractal structures with multiple structural levels. This model provides shape-independent parameters such as the radii of gyration and scaling exponents which are associated to the fractal dimension.[47] Further details on the model and the corresponding equations may be found in the SI file.

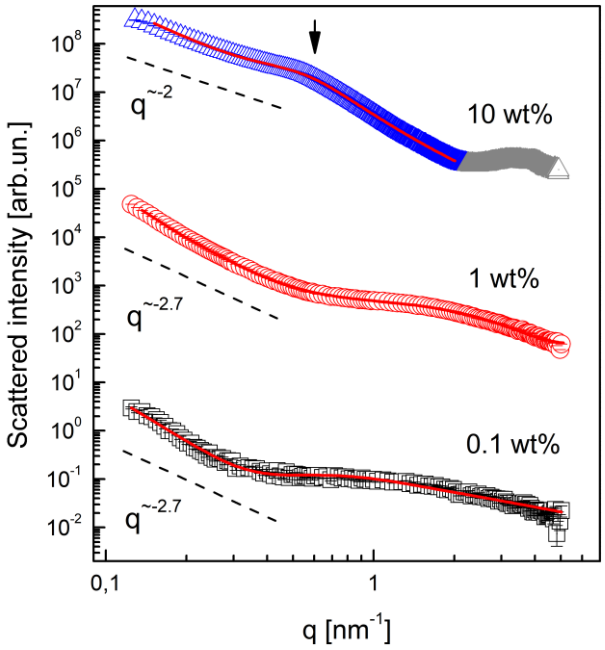

Figure 1: SAXS data from samples containing peptides at different concentrations. Solid red lines are fits performed with the models indicated in text. The black arrow in the upper curve indicates an interference peak arising from interparticle correlations whereas the gray region provides information on the inner structure of peptide fibers.

The data reveal that the large-scale objects have characteristic radii of gyration of 42.8 and 63.0 nm, respectively, for solutions containing 0.1 wt% and 1 wt% peptide. The dimensionality of the objects appears to be not strongly affected at this concentration range since the Porod exponent *P* values remain close to 3, consistent with rough surface fractals.[46] The more interesting results are related to the inner structure of the aggregates, with radii of gyration equal to 4.0 and 5.5 nm for sub-particles in samples with 0.1 wt% and 1 wt% peptide. The dimensionalities of these subunits were found to be 0.37 and 0.22, respectively, and their proximity to a Porod exponent equal to 0 suggests the presence of globular shapes in the inner structure of the aggregates.[44]

Data from samples prepared at the highest concentration investigated (10 wt%) exhibit SAXS profiles quite different in comparison with their more diluted counterparts. The macroscopic behavior of these samples is peculiar, with appearance of a gel phase over the course of a few days, and such contrast is also observed at the nanometer scale. Polarizing optical microscopy images from samples at this concentration reveal the presence of large birrefringent domains, also indicating local ordering of anisotropic particles (SI Fig.S3). The most remarkable feature in the scattering curves from these formulations is the presence of an interference peak at the intermediate *q*-range, close to $q = 0.5$ nm^{-1}, arising from correlation between particles in the medium. Also, the high-*q* range, $q > 2$ nm^{-1}, exhibits a diffuse peak at q ~ 4 nm^{-1} which arises from the inner structure of the particles in the gel (see fXRD discussion below). In addition, the scaling exponents either at low-*q* or at intermediate-to-high-*q* regions are clearly distinct than those observed previously, also suggesting modifications in the shape of the particles. The complicated SAXS profile, with appearance of an interference peak in the middle of the data and the presence of different structural levels in the profiles, makes it very complex to perform full-range fitting using analytical models.[49] Thus, to describe structural features of the samples, we adopted an empirical approach combining a simple power-law decay and the Teubner-Strey model.[49, 50] This model is often used for describing scattering from micro-emulsions and it provides quantitative information on average distances and correlation lengths between scattering domains within bi-continuous networks.[50] Further details on the

model appear in the SI file. The fitting procedure (see SI file) shows the presence of a scaling exponent ~ 2.66, indicating that the local structure of the aggregates – i.e., the inner part of the peptide fibers sustaining the gel (see AFM imaging below) - is composed of mass-fractal objects, in agreement with morphology of the particles found in more diluted solutions. On the other hand, the average separation between scattering domains is found to be d = 13.0 nm, with correlation lengths ξ = 3.66 nm, suggesting weakly-correlated domains across the sample.

To get further insights into the structure of the self-assemblies, fiber X-ray diffraction (*fXRD*) was carried out on aligned stalks prepared from dried 10 wt% samples. An oriented pattern is shown in Figure 2A, revealing clear cross-β-like features. The pattern is characterized by a set of sharp diffraction peaks along the equator with repeat distances appearing at d_{exp} = 2.21, 1.55, 1.11 and 0.40 nm. The reduced pattern, with the angular positions of the peaks is shown in Figure 2B.

The first and second peaks on the equator are consistent with broad Bragg reflections in the SAXS profiles from 10 wt% solutions (see upper curve in Figure 1), indicating that they are associated with highly-ordered structures with repeat distances observed under hydrated conditions. A diffuse arc at d_{exp} = 0.66 nm completes the series of equatorial reflections. In the perpendicular direction, along the meridian, the pattern is marked by very strong arcs located at d_{exp} = 0.48 nm. This repeat distance arises from the spacing between β–strands held together by H-bonds within β–sheets running along the fibril axis.[51, 52] These features are classical cross–β signatures of molecular packing of aggregates and makes these assemblies structurally similar to the organization often found in amyloidogenic peptides.[53] A shallow diffraction ring is also found at d_{exp} = 0.56 nm, bringing a total of seven observable reflections in the pattern.

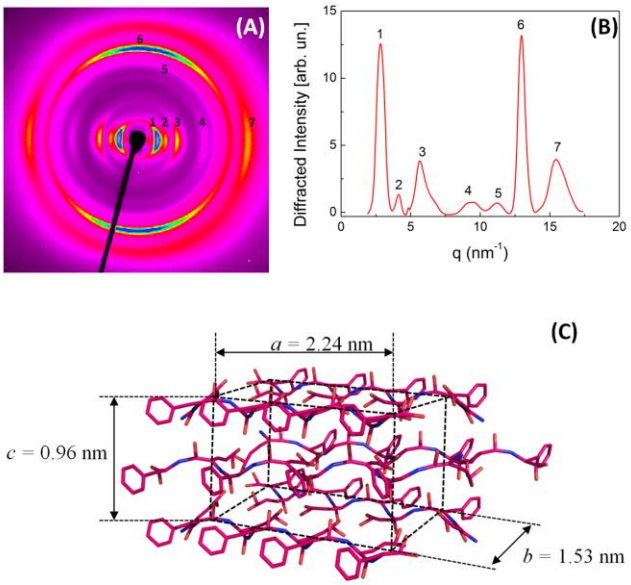

Figure 2: (A) *fXRD* pattern from an oriented stalk dried from a 10 wt% peptide solution. (B) Radial average of the diffraction pattern showing the corresponding peak positions in terms of scattering vectors. (C) Schematic model showing molecular packing within the unit cell.

We performed dozens of trials using the unit cell optimization module available within the software CLEARER[39] to provide peak indexation for assemblies; however, unequivocal assignment was not possible since many solutions with very different lattice parameters led to reasonable predictions of the seven reflections appearing in the pattern. The unit cell providing the minimum difference between predicted (d_{calc}) and experimental (d_{exp}) peaks was an orthorhombic cell with lattice parameters a = 2.24, b = 1.55 and c = 0.96 nm. In this case, the average error was found at 2 × 10^{-3} %, and a comparison between theoretical and experimental data is presented in Table S2, along with the corresponding Miller indices. The orthorhombic symmetry and the cross–β organization are in agreement with previous results on alternating arginine/phenylalanine octapeptides.[15] Based on this least-error unit cell, we were able to propose a simplified structural model sketched in Figure 2C. The parameter c = 0.96 nm accounts for repeat distances across the fibril axis and it is twice the separation between anti-parallel strands. The distance between sheets is given by the lattice parameter b = 1.55 nm and it is consistent with extended glutamic acid chains intercalating Na^+ counter-ions layers that presumably screen electrostatic repulsions in the interstice of the structure. Finally, the

parameter a = 2.24 nm is parallel to the axis of the strands and it is consistent with slightly folded backbones. Indeed, the size of an extended octameric peptide chain adopting an antiparallel β-sheet structure is *ca.* 8 × 0.34 = 2.72 nm and accommodation into a 2.24 nm long unit cell requires a compression of about 18% or a certain extent of interdigitation.

AFM: Topography Investigations

Ultrastructural characterization of peptide aggregates was carried out through AFM imaging on samples dried from solutions prepared at concentrations used in SAXS experiments. In Figure 3A, the topography of a sample obtained from a 0.1 wt% solution deposited onto freshly-cleaved mica reveals the dominant presence of small aggregates with irregular shapes. Typical lateral sizes are found in the range 30 - 60 nm, consistent with the macrostructural gyration radius derived from the Beaucage model used to fit SAXS data (see Table 1), whereas heights appear to be much smaller with dimensions close to ~1.5 nm, similar to the *b* direction of the unit cell revealed by fXRD assays. These findings suggest that these small aggregates are made from a few peptide chains laterally-associated to form oligomeric species.

In samples prepared from more concentrated solutions, morphology changes dramatically and new levels of organization appear in the aggregates. For 1 wt% peptide solutions, Figure 3B, nanostructures are characterized by long fibrils with lengths easily reaching the micrometer scale. The diameters of the fibrils have been estimated to be ~ 35 nm, consistent with lateral dimensions measured in particles found in low-concentration samples. Therefore, our AFM data are consistent with fibrils made up from subunits of coalesced oligomers. It is important to highlight that SAXS data from solutions containing peptides at this same concentration are consistent with the presence of larger oligomers, suggesting that fibrils appear in the AFM images as a consequence of the drying process during sample preparation. The fibrils appear associated into bundles, forming long flat tapes with cross-section sizes easily reaching a few hundred nanometers (see inset in Figure 3B) suggesting that self-assembly follows a hierarchical framework. Figure 3C shows the topography of a sample prepared from a gelled solution containing 10 wt% peptide. An intricate network is evident, which is composed

of thicker fibers forming a cross-linked matrix able to host the aqueous phase in the interstices. At such a high concentration, fiber bundles appear consolidated into mature structures with diameters of the order of ~300 nm, consistent with the presence of highly-intertwined assemblies. Additional AFM images are shown in Figures S4-S6.

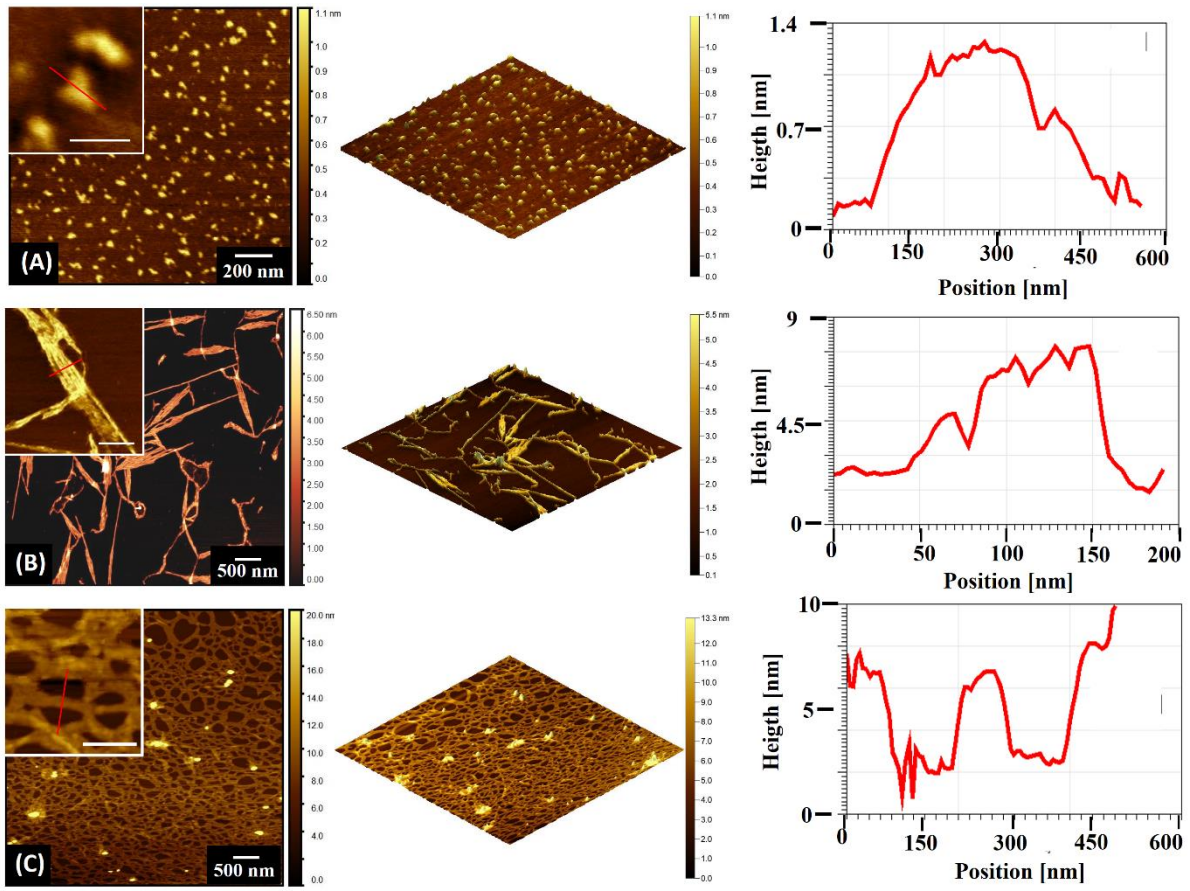

Figure 3: Left and centre columns: Topography images from peptide samples dried from solutions prepared at different concentrations: (A) 0.1 wt%; (B) 1 wt% and (C) 10 wt%. Right column: height profiles across the lines shown in the left-hand topography images.

FTIR: probing the presence of β_2-sheets

A major characteristic of glutamic acid-rich oligopeptides is the formation of amyloid-like self-assemblies organized into the so-called β_2-type structure.[27] This structure is characterized by crossed *H*-bonds formed between carboxyl groups in glutamic acid side-chains and NH in amide bonds along the backbones of β–strands in adjacent sheets.[26, 27] In this section, we provide further information on the secondary structure of the assemblies in order to assess the presence of β_2-structures at play in the maintenance of aggregates described here. For this, we have combined information from FTIR assays carried out in bulk liquid samples and nanoscale IR spectroscopy performed directly on discrete nanostructures deposited onto dried substrates.

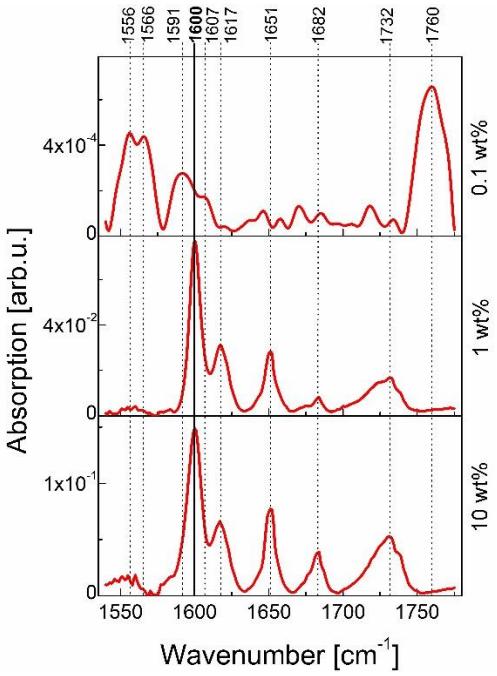

Figure 4: FTIR spectra from peptide solutions at concentrations indicated. Dotted lines are guides for the eyes indicating the positions of main peaks appearing in the spectra. The mode at 1600 cm^{-1}, associated to β_2-sheets,[24-27] is highlighted in bold.

Figure 4 shows FTIR data from solutions containing peptides at the concentrations previously investigated by SAXS and AFM. These samples have been prepared using deuterated water to minimize overlapping between the intense mode due to water bending vibration near 1640 cm^{-1} and peptide peaks in the middle of the amide I band.[55-57] A clear

concentration-dependent behavior is found in the data as indicated by remarkable contrast observed between the spectral signature from samples prepared at 0.1 wt% and those from their more concentrated counterparts. Profiles from dilute solutions (upper curve in Figure 4) are characterized by strong vibrations at 1556 and 1566 cm^{-1}, which are assigned to antisymmetric stretching of COO^- groups at glutamic acid side chains.[56,57] A doublet at positions 1591 and 1607 cm^{-1} is ascribed to stretching of C-C bonds in phenylalanine aromatic rings,[57] whereas another intense band at 1760 cm^{-1} accounts for stretching of C=O bonds in glutamic acid side chains. In the amide I region, minor peaks appear at 1645 and 1670 cm^{-1}, being tentatively ascribed to small fractions of random coil and β–turn conformations.[56]

In the case of samples prepared at higher peptide concentrations, 1 and 10 wt%, the profiles are strongly different, and spectra are clearly dominated by amide I vibrations consistent with the presence of higher degree of order and the formation of stable secondary structures. Infrared spectra from these samples are featured by a very strong peak centered at 1600 cm^{-1} that is recognized as a signature of β_2-sheet structures.[25, 27] This vibration is usually interpreted as a red-shifted amide I peak involving the stretching of carbonyl groups where the oxygen behaves as an acceptor center in two (bifurcated) H-bonds simultaneously.[27, 54] Unlike conditions usually adopted elsewhere, with self-assembly occurring in acidic medium under severe heating (up to 90 °C),[24, 25] samples herein have been prepared in alkaline medium and have only undergone moderate heating for a short time period, demonstrating that our $[EF]_4$ sequences are capable of forming β_2-type structures even under mild conditions. The presence of a sharp peak at 1617 cm^{-1} indicates that β_1 structure – i.e., β-sheets held together by "standard" H-bonds between carbonyl and amide NH groups at adjacent sheets – is also present in a lower fraction. The presence of some unordered structures is indicated by a noticeable vibration at 1650 cm^{-1}, and β-turn conformations are suggested shallow band at 1673 cm^{-1}. A resonance at 1682 cm^{-1} is indicative of anti-parallel strands, in agreement with XRD data shown above. Other peaks appearing at 1722, 1732 and 1742 cm^{-1} are related to the acid glutamic side-chains and are associated to vibrations in the carbonyl group.[55]

AFM-IR: infrared spectra from individual nanoparticles

Infrared nanospectroscopy was combined with AFM on dried samples to provide spatially-resolved data of the assemblies at the nanoscale. The advantage of this approach is that it yields single-particle spectra,[41] in contrast to average information derived from bulk FTIR spectra discussed above. Figure 5 shows AFM images from nanoparticles obtained from solutions prepared at 0.1 wt% and 10 wt% peptide, alongside with infrared data collected on the from individual assemblies. The size of the region probed during infrared scans was limited by the AFM tip diameter, here ~ 30 nm.[40] From the data, it is evident that vibrational profiles on dried assemblies are quite different from infrared signatures observed in peptide solutions suggesting that dehydration followed by loss of solvent molecules mediating H-bonds in the interstice of the assemblies are associated to changes in the secondary structure.

In Figures 5A and B, nanospectroscopy data from globular particles obtained from a 0.1 wt% peptide solution are shown. Spectra from different aggregates in the sample exhibit the same general feature, with a strong vibration at 1628 cm^{-1} revealing the presence of standard β–sheet conformers. In some particles (curves 1-4, in Figure 5B), it is possible to identify shallow peaks at 1560 and 1608 cm^{-1}, which are tentatively assigned to COO^- and C-C stretching, respectively, of glutamic acid and phenylalanine side chains.[39] These findings contrast with data from hydrated samples, which are characterized by low-intensity peaks across the amide I region (see Figure 4, upper curve), suggesting that more organized superstructures appear in the aggregates upon release of solvent.

Figures 5C and 5D show nanospectroscopy data from self-assemblies on samples prepared using a 10 wt% peptide solution. The data are more complex and spectra from nanostructures with different morphologies show distinct infrared signatures. A spectrum collected on a round polymorph (curve 1 in 5D) is characterized by strong peaks at 1564 and 1580 cm^{-1}. A shoulder at 1600 cm^{-1} is consistent with the presence of some β_2 content and a noticeable band at 1642 cm^{-1} indicates that considerable fractions of β_1 conformations are also present in the aggregate.[55] On the other hand, spectra collected along peptide fibers (curves 2-7

in 5D) display a larger number of resonances across the amide I range, with appearance of intense peaks at 1648 and 1672 cm^{-1}. This information indicates that the secondary structure in fibers exhibits higher levels of organization compared to oligomer species self-assembled into round aggregates, in agreement with previous findings on amyloidogenic assemblies.[53] The band at 1648 cm^{-1} is ambiguous and it could be interpreted either as an evidence for α–helix or an indication for random coil structures; however, since our peptides are short and comprise alternate hydrophobic and polar residues along the backbone, α-helices are not favored and random coil conformations are more likely in the assemblies. The infrared signature of TFA counterion is characterized by a sharp peak centered at 1673 cm^{-1} due to the strong vibration of COO^- groups.[58,59] Peptides used here were provided in the ammonium salt form; thus, residual TFA from synthesis is not an issue in our samples. By examining FTIR data from our solutions, Figure 4, one observes that strong peaks at 1673 cm^{-1} are absent and vibrations at ~ 1670 cm^{-1} are marginally found in the spectra. In this case, we ascribe the peak at 1672 cm^{-1} to anti-parallel β-sheets organized into β_1-type conformations in the fibers,[59] corroborating our previous XRD data which revealed the presence of β–sheets on dried fibers. Putting the findings above together, comparison between infrared nanospectroscopy and FTIR information from peptide solutions indicates destabilization of β_2 structures upon drying, accompanied by growth of β_1 and disordered content. In fact, since bifurcated H-bonds are energetically weaker than regular H-bonds,[54] appearance of standard β-sheets is likely favored upon dehydration. Chemical maps from samples shown in Figure 5 are presented in Figures S7 and S8 (SI file) and they show that absorption related to β_2 structures is weaker in comparison to vibrations related to β_1 conformers.

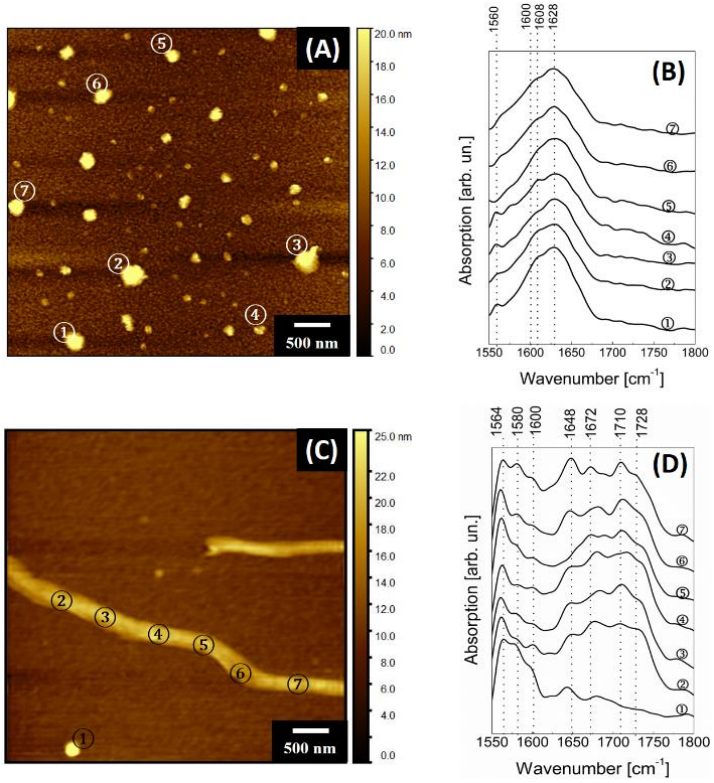

Figure 5: Infrared nanospectroscopy images and spectra from self-assemblies obtained from solutions prepared at 0.1 wt% (A and B) and 10 wt% peptide (C and D). Numbered circles are placed closer to the nanoparticle on the top of which individual spectra were collected.

To further investigate changes introduced by dehydration on infrared profiles of glutamic acid-rich self-assemblies, we performed single-particle nanospectroscopy in self-assemblies obtained from a 1 wt% peptide solution. As revealed by AFM imaging above, nanostructures in samples at this concentration exhibit tape-like morphologies (Figure 6) and they are composed of fibrillar subunits. Infrared spectra shown in Figure 6A reveal that, although peaks at ~ 1600 cm^{-1} are still visible, bands at 1630 cm^{-1} are stronger for most of the spectra collection points, similar to the behavior observed in globules found in more diluted samples (Figure 5A and B). This observation suggests that higher fractions of standard β_1 species are present in the tapes, also contrasting with predominance of β_2-structures observed in peptide solutions. The spectra also exhibit a peak at 1562 cm^{-1}, which is assigned to antisymmetric stretching of $–COOH^-$ groups,[27] and the diffuse band centered at 1690 cm^{-1} is consistent with anti-parallel β-sheets.[56] Comparing spectra from nanotapes in Figure 6A and fibers in Figure 5D, one observes that infrared profiles from tape-like structure exhibit a lower

number of resonances, indicating that a lower degree of supramolecular ordering is present in these assembles.

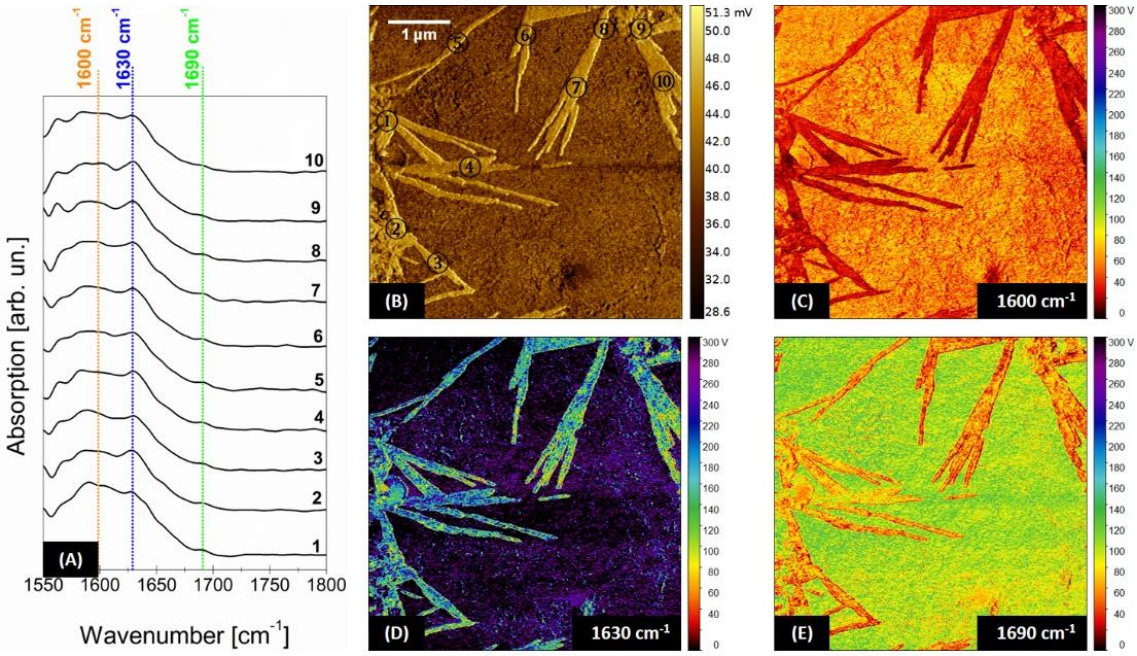

Figure 6: Nanospectroscopy from a 1 wt% dried peptide solution originally dissolved in D_2O. (A) infrared spectra from different regions of individual peptide nanotapes; (B) lateral deflection image showing morphology of nanotapes on the top of an amorphous film. Numbered circles indicate the location where spectra shown in (A) were collected. (C), (D) and (E) Infrared adsorption maps collected, respectively, at 1600 cm^{-1}, 1630 cm^{-1} and 1690 cm^{-1}.

Another powerful feature of nanoscale IR spectroscopy is providing chemical images with nanoscopic resolution through collection of infrared absorption maps.[38, 60, 61] The unique morphology of the tapes, where flat structures exhibit distinguishable subunits, allows chemical images with a finer level of spatial detail to be obtained. In our experiments, we have collected infrared images at 1600 cm^{-1}, 1630 cm^{-1} and 1690 cm^{-1}. These absorption wavenumbers have been chosen because they are correlated to β_2 (1600 cm^{-1}) and common β-sheet structures (1630 and 1690 cm^{-1});[27, 56] thus, by inspecting chemical maps obtained at these characteristic bands, we have been able to qualitatively examine the spatial distribution of different types of β-sheets across the nanotapes. In Figures 6C-E, absorption maps at different wavenumbers are exhibited to provide direct comparison between different spectral bands and they reveal that infrared

intensities are clearly weaker in maps collected at 1600 cm^{-1} (Figure 6C). In addition, at this wavenumber, absorption is homogeneously distributed across the nanotapes, indicating β_2 structures uniformly spread along the nanoparticles. In Figure 6D, maps collected at 1630 cm^{-1}, correlated to β-sheet conformations formed between carbonyl and amide NH groups at adjacent sheets, show stronger absorption than that associated to β_2-type structures, corroborating that β_1 organization is predominant in dried nanotapes. A similar behavior is found for images collected at 1690 cm^{-1} related to anti-parallel conformation (see Figure 6E). The maps exhibit inhomogeneities identified by different color zones across the aggregates which are interpreted as an indication for clusters containing distinct fractions of secondary structures. Particularly, intense adsorption zones are observed corresponding to striated lines parallel to the long axis of the tapes indicating that the core of fibrillar subunits is richer in β_1 structures. A possible explanation for the higher uniformity in distribution of zones associated to β_2 conformers could be that bifurcated H-bonding is driven by carbonyl groups on glutamic acid side-chains. During self-assembly in water, these hydrophilic side-chains tend to be located close to the solvent interface whereas peptide backbones responsible for β-sheet pairing remain buried in the core of the structure. Indeed, as indicated by XRD data discussed above, paired β-strands form galleries running parallel to the long axis of the fibrils, in close agreement with striated marks revealed in the infrared adsorption maps.

CONCLUSIONS

The simplified models investigated here, where acid glutamic residues appear intercalated with phenylalanine residues, mimic a class of peptide sequences with prominent role in biological processes, including immune and glutamatergic systems. Several amyloidogenic features of the self-assemblies were demonstrated and AFM and SAXS experiments indicated the formation of small oligomers whose coalescence into nanofibrils leads to production of mature fibers and nanotapes. A concentration-dependent polymorphism was found, with appearance of fractal-like oligomers in diluted formulations proceeding to

development of nanotapes and nanofibers in presence of higher peptide concentrations. Such a complex behavior required empirical models to describe the scattering data. In this case, Beaucage and Teubner-Strey form factors showed the presence of multi-level organization in the self-assemblies with predominance of fractal structures in solution. The presence of birrefringent domains in gels showed the local orientation of anisotropic nanostructures and this macroscale feature is the result of hierarchical order extending from peptide packing at the nanoscopic level.

A particular feature of glutamic acid-rich sequences is organization into β_2-sheets,[27] a structural pattern characterized by bifurcated *H*-bonds formed between carboxyl groups at acid glutamic side-chains and amide NH along the backbones of β–strands at adjacent sheets.[26, 27] The presence of β_2 conformers in our study was revealed by infrared spectroscopy and this conformation was found to be the dominant fraction in hydrated samples, as revealed by a very intense red-shifted amide I peak at 1600 cm^{-1}. Single-particle spectroscopy was carried out to provide direct IR mapping from individual assemblies. To our knowledge, this is the first study using direct nanoscale IR measurements to probe the formation of β_2 structures in glutamic acid-rich peptide aggregates. A notable result arising from these experiments is a remarkable decrease of the fraction of β_2-sheets observed upon drying. Destabilization of β_2 structures was observed for all concentrations and polymorphs in our study and a progressive degree of order was found depending on peptide concentration, with globular aggregates exhibiting a lower degree of order, followed by nanotapes at an intermediate stage and mature fibers showing the highest complexity in their spectra with a larger number of resonances associated to chemical bonds across the amide I region. We propose that this β_2-to-β_1 transition is a consequence of the release of water from the interstices of peptide assemblies, where solvent molecules mediate H-bonds. Since energies involved in the stabilization of bifurcated H-bonds are lower in comparison to "standard" H-bonds,[54] appearance of β_1 conformers is likely favored upon dehydration. Chemical maps obtained at wavenumbers corresponding to the spectral signature of the different types of β-sheets enabled us to examine the spatial distribution of these

structures across the nanoparticles. These maps displayed β_2-type structures homogeneously spread along nanotapes and β_1 conformation concentrated in striated patterns parallel to the long axis of the tapes, indicating that the core of the fibrillar subunits is likely richer in this kind of conformer. It is also important to stress the role of phenylalanine residues in the self-assembly presented here. In fact, the propensity of aromatic side chains at adjacent strands to establish π–π interactions likely favors the growth of β–sheets where peptide strands appear perpendicularly to the long axis of the supramolecular arrangement. These characteristics are critical for appearance of the cross–β structure revealed by our diffraction data and they are consistent with the organization previously found in intercalating arginine/phenylalanine oligopeptides.[15,16,62]Therefore, the anionic peptides investigated here show amyloidogenic features in line with their cationic (argininic) analogs, corroborating the importance of Phe residues in the formation of amyloid-like nanostructures.

Summarizing, we have elucidated the structure of peptide aggregates built up from short peptides comprising alternating glutamic acid moieties and phenylalanine. A sophisticated combination of techniques unequivocally showed the formation of amyloid species and secondary structure was found to present major fractions of β_2-sheets. Direct infrared measurements carried out on the surface of individual nanoparticles showed that β_2-type structures are the dominant form only under hydrated conditions, which points to the major role of water molecules in the stabilization of β_2 conformations. Dehydration leads to disruption of bifurcated H-bonds and destabilization of β_2-type networks.

ACKNOWLEDGEMENTS

This work was supported by FAPESP under grant n° 2016/24409-3 (Regular-Support funding granted to ERS). LRM is recipient of a MSc. fellowship from CAPES-PROEX scheme granted to the Graduate Program in Molecular Biology of the Federal University of Sao Paulo. IWH thanks EPSRC (UK) for the award of a Platform Grant (ref. EP/L020599/1). WAA is supported by the National Council for Scientific and Technological Development (CNPq grant no.

302923/2015-2), the National Institute of Science and Technology in Bioanalytics (FAPESP grant no. 2014/50867-3 and CNPq grant no. 465389/2014-7), and the São Paulo Research Foundation (FAPESP grant nos. 2015/24018-1, 2017/02317-2). SAXS data were collected at LNLS under proposal 20160420. Carlos Costa and Evandro Manzoni are kindly acknowledged for assistance during AFM experiments at LNNano (proposal numbers: AFM21086 and AFM22077). Prof. Juliana Souza (at UFABC) is kindly acknowledged for providing access to FTIR instrument. ERS is recipient of a CNPq fellowship (n° 307017/2016-8).

REFERENCES

1. Hosseinkhani H, Hong PD, Yu DS. Self-Assembled Proteins and Peptides for Regenerative Medicine. *Chem. Rev.* **2013;** *113* (7): 4837-4861.
2. Wei G, Su Z, Reynolds NP, Arosio P, Hamley IW, Gazit E, Mezzenga R. Self-assembling peptide and protein amyloids: from structure to tailored function in nanotechnology. *Chem. Soc. Rev.* **2017;** 46:4661-4708.
3. Sun L, Zheng C, Webster T. J. Self-assembled peptide nanomaterials for biomedical applications: promises and pitfalls. *Int. J. Nanomed.* **2017;** *12:* 73-86.
4. Panettieri S, Ulijn R. V. Energy landscaping in supramolecular materials. *Curr. Opin. Struc. Biol.* **2018;** *51:* 9-18.
5. Tantakitti F, Boekhoven J, Wang X, Kazantsev RV, Yu T, Li J, Zhuang E, Zandi R, Ortony JH, Newcomb CJ, Palmer LC, Shekhawat GS, de la Cruz M. O, Schatz GC, Stupp SI. Energy landscapes and functions of supramolecular systems. *Nature Materials* **2016;** *15:* 469-476.
6. Ricchiuto P, Brukhno AV, Auer S. Protein Aggregation: Kinetics versus Thermodynamics. *J. Phys. Chem. B* **2012;** *116* (18): 5384-5390.
7. Place ES, Evans ND, Stevens MM. Complexity in biomaterials for tissue engineering. *Nature Materials* **2009;** *8:*457-470.
8. Maude S, Tai LR, Davies RP, Liu B, Harris SA, Kocienski PJ, Aggeli A. Peptide synthesis and self-assembly. *Top. Curr. Chem.* **2012;** *310:* 27-69.
9. Dehsorkhi A, Castelletto V, Hamley IW. Self-assembling amphiphilic peptides. *J. Pep. Sci.,* **2014;** *20* (7): 453-467.
10. Chiti F, Dobson C. M. Protein misfolding, functional amyloid, and human disease. *Annu. Rev. Biochem.* **2006;** *75:* 333-366.
11. Tjernberg LO, Callaway DJE, Tjernberg A, Hahne S, Lilliehook C, Terenius L, Thyberg J., Nordstedt C. A molecular model of Alzheimer amyloid beta-peptide fibril formation. *J. Biol. Chem.* **1999;** *274* (18): 12619-12625.
12. Tjernberg LO, Naslund J, Lindqvist F, Johansson J, Karlstrom AR, Thyberg J, Terenius L, Nordstedt C. Arrest of beta-amyloid fibril formation by a pentapeptide ligand. *J. Biol. Chem.* **1996;** *271* (15): 8545-8548.
13. Tjernberg L, Hosia W, Bark N, Thyberg J, Johansson J. Charge Attraction and β Propensity Are Necessary for Amyloid Fibril Formation from Tetrapeptides. *J. Biol. Chem.* **2002;** *277* (45): 43243-43246.

14. Krysmann MJ, Castelletto V, Kelarakis A, Hamley IW, Hule RA, Pochan DJ. Self-assembly and hydrogelation of an amyloid peptide fragment. *Biochemistry* **2008;** *47* (16): 4597-605.
15. Decandio CC, Silva ER, Hamley IW, Castelletto V, Liberato MS, Oliveira VX, Oliveira CLP, Alves WA. Self-Assembly of a Designed Alternating Arginine/Phenylalanine Oligopeptide. *Langmuir* **2015;** *31* (15): 4513-4523.
16. Liberato MS, Kogikoski S, Silva ER, Silva RH, Oliveira VX, Scott LP, Ando RA, Coutinho-Neto MD, Alves WA. Self-Assembly of Arg-Phe Nanostructures via the Solid-Vapor Phase Method. *J. Phys. Chem. B* **2013;** *117:* 733-740.
17. Silva ER, Cooney G, Hamley IW, Alves WA, Lee S, O'Connor B F, Reza M, Ruokolainen J, Walls D. Structural behaviour and gene delivery in complexes formed between DNA and arginine-containing peptide amphiphiles. *Soft Matter* **2016;** *12* (45): 9158-9169.
18. Hamley IW. Small Bioactive Peptides for Biomaterials Design and Therapeutics. *Chem. Rev.,* **2017;** *117* (24): 14015-14041.
19. da Silva ER, Alves WA, Castelletto V, Reza M, Ruokolainen J, Hussain R, Hamley IW. Self-assembly pathway of peptide nanotubes formed by a glutamatic acid-based bolaamphiphile. *Chem. Comm.* **2015,** *51* (58), 11634-11637.
20. Chelius D, Jing K, Lueras A, Rehder DS, Dillon TM, Vizel A, Rajan RS, Li T, Treuheit MJ, Bondarenko PV. Formation of Pyroglutamic Acid from N-Terminal Glutamic Acid in Immunoglobulin Gamma Antibodies. *Anal. Chem.* **2006;** *78* (7): 2370-2376.
21. Yu L, Vizel A, Huff MB, Young M, Remmele RL, He B. Investigation of N-terminal glutamate cyclization of recombinant monoclonal antibody in formulation development *J. Pharm. Biomed. Anal.,* **2006;** *42* (4): 455-463.
22. Purwaha P, Silva LP, Hawke DH, Weinstein JN, Lorenzi PL. An Artifact in LC-MS/MS Measurement of Glutamine and Glutamic Acid: In-Source Cyclization to Pyroglutamic Acid. *Anal. Chem.* **2014;** *86* (12): 5633-5637.
23. Marsden HR, Handgraaf JW, Nudelman F, Sommerdijk NA, Kros A. Uniting polypeptides with sequence-designed peptides: synthesis and assembly of poly(gamma-benzyl L-glutamate)-b-coiled-coil peptide copolymers. *J. Am. Chem. Soc.* **2010;** *132* (7): 2370-2377.
24. Tobias F, Keiderling TA. Role of Side Chains in β-Sheet Self-Assembly into Peptide Fibrils. IR and VCD Spectroscopic Studies of Glutamic Acid-Containing Peptides. *Langmuir* **2016;** *32* (18): 4653-4661.
25. Chi H, Welch WRW, Kubelka J, Keiderling TA. Insight into the Packing Pattern of β2 Fibrils: A Model Study of Glutamic Acid Rich Oligomers with 13C Isotopic Edited Vibrational Spectroscopy. *Biomacromol.* **2013;** *14* (11): 3880-3891.
26. Fulara A, Hernik A, Nieznańska H, Dzwolak W. Covalent Defects Restrict Supramolecular Self-Assembly of Homopolypeptides: Case Study of β2-Fibrils of Poly-L-Glutamic Acid. *PLoS One* **2014;** *9* (8): e105660.
27. Fulara A, Dzwolak W. Bifurcated Hydrogen Bonds Stabilize Fibrils of Poly(l-glutamic) Acid. *J. Phys. Chem. B* **2010;** *114* (24): 8278-8283.
28. Sugimoto Y, Yatsunami K, Tsujimoto M, Khorana HG, Ichikawa A. The amino acid sequence of a glutamic acid-rich protein from bovine retina as deduced from the cDNA sequence. *Proc. Natl. Acad. Sci. U.S.A.* **1991;** *88* (8): 3116-3119.
29. Dick LW, Kim C, Qiu DF, Cheng KC. Determination of the origin of the N-terminal pyro-glutamate variation in monoclonal antibodies using model peptides. *Biotechnol. Bioeng.* **2007;** *97* (3): 544-553.
30. Li W, Joshi MD, Singhania S, Ramsey KH, Murthy AK. Peptide Vaccine: Progress and Challenges. *Vaccines* **2014;** *2* (3): 515-536.
31. Sanacora G, Zarate CA, Krystal JH, Manji HK. Targeting the glutamatergic system to develop novel, improved therapeutics for mood disorders. *Nat. Rev. Drug Discovery* **2008;** *7(5):* 426-437.

32. Wang BP, Wang ZL, Sun L, Yang L, Li HM, Cole AL, Rodriguez-Rivera J, Lu HC, Zheng H. The Amyloid Precursor Protein Controls Adult Hippocampal Neurogenesis through GABAergic Interneurons. *J. Neurosci.* **2014;** *34* (40): 13314-13325.
33. Tong HC, Zhang XP, Meng XJ, Xu PY, Zou XM, Qu SG. Amyloid-beta peptide decreases expression and function of glutamate transporters in nervous system cells. *Int. J. Biochem. Cell Biol.* **2017;** *85:* 75-84.
34. Treusch S, Hamamichi S, Goodman JL, Matlack KES, Chung CY, Baru V, Shulman JM, Parrado, A, Bevis, B. J, Valastyan, J. S, Han, H, Lindhagen-Persson, M, Reiman, E. M, Evans, D. A, Bennett DA, Olofsson A, DeJager PL, Tanzi RE, Caldwell KA, Caldwell GA, Lindquist S. Functional Links Between A beta Toxicity, Endocytic Trafficking, and Alzheimer's Disease Risk Factors in Yeast. *Science* **2011;** *334* (6060): 1241-1245.
35. Gallivan JP, Dougherty DA. Cation-Pi Interactions in Structural Biology. *Proc. Natl. Acad. Sci. U S A* 1999; **96**: 9459–9464.
36. Tamamis P, Adler-Abramovich L, Reches M, Marshall K, Sikorski P, Serpell L, Gazit E, Archontis G. Self-Assembly of Phenylalanine Oligopeptides: Insights from Experiments and Simulations. *Biophys J* 2009; **96**: 5020–5029.
37. Beck A, Bussat MC, Klinguer-Hamour C, Goetsch L, Aubry JP, Champion T, Julien E, Haeuw JF, Bonnefoy JY, Corvaia N. Stability and CTL activity of N-terminal glutamic acid containing peptides. *J. Pep. Res.* **2001;** *57* (6): 528-538.
38. Bressler I, Kohlbrecher J, Thunemann AF. SASfit: a tool for small-angle scattering data analysis using a library of analytical expressions. *J. Appl. Crystallog.* **2015;** *48* (5): 1587-1598.
39. Makin OS, Sikorski P, Serpell L C. CLEARER: a new tool for the analysis of X-ray fibre diffraction patterns and diffraction simulation from atomic structural models. *J. Appl. Crystallog.* **2007;** *40:* 966-972.
40. Dazzi A, Prater CB. AFM-IR: Technology and Applications in Nanoscale Infrared Spectroscopy and Chemical Imaging. *Chem. Rev.* **2017;** *117* (7): 5146-5173.
41. Dazzi A, Saunier J, Kjoller K, Yagoubi N. Resonance enhanced AFM-IR: A new powerful way to characterize blooming on polymers used in medical devices. *Int. J. Pharm.* **2015;** *484* (1-2): 109-114.
42. Aguiar J, Carpena P, Molina-Bolívar JA, Carnero Ruiz C. On the determination of the critical micelle concentration by the pyrene 1:3 ratio method. *J. Colloid Interf. Sci.* **2003;** *258* (1): 116-122.
43. Castelletto V, Cheng G, Greenland BW, Hamley IW, Harris, PJ. Tuning the Self-Assembly of the Bioactive Dipeptide l-Carnosine by Incorporation of a Bulky Aromatic Substituent. *Langmuir* **2011;** *27* (6): 2980-2988.
44. Hammouda B. A new Guinier-Porod model. *J. Appl. Crystallog.* **2010;** *43* (4): 716-719.
45. Pedersen JS. Analysis of small-angle scattering data from colloids and polymer solutions: modeling and least-squares fitting. *Adv. Coll.Interf. Sci.* **1997;** *70* (0): 171-210.
46. Beaucage, G. Small-angle scattering from polymeric mass fractals of arbitrary mass-fractal dimension. *J. Appl. Crystallog.* **1996;** *29:*134-146.
47. Beaucage, G. Approximations leading to a unified exponential power-law approach to small-angle scattering. *J. Appl. Crystallog.* **1995;** *28:* 717-728.
48. Zemb T, Lindner P. *Neutrons, X-rays and light: scattering methods applied to soft condensed matter*; 1st ed, Elsevier: Amsterdam; Boston, 2002. p x, 541 p.
49. Hammouda, B. Clustering in polar media. *J. Chem. Phys.* **2010;** *133* (8): 084901.
50. Kogikoski S, Liberato MS, Factori IM, Silva ER, Oliveira, CLP, Ando R.A, Alves WA. Polycaprolactone-Polyaniline Blend: Effects of the Addition of Cysteine on the Structural and Molecular Properties. *J. Phys. Chem. C, **2016;** 121* (1): 863-877.
51. Teubner M, Strey R. Origin of the Scattering Peak in Microemulsions. *J. Chem. Phys.* **1987;** *87* (5): 3195-3200.
52. Jahn T R, Makin OS, Morris KL, Marshall KE, Tian P, Sikorski P, Serpell LC. The Common Architecture of Cross-beta Amyloid. *J. Mol. Biol.* **2010;** *395* (4): 717-727.

53. Serpell L. Amyloid structure. *Essays Biochem.* **2014;** *56:* 1-10.
54. Hamley IW. Peptide fibrillization. *Angew. Chem. Int. Ed. Engl.* **2007;** *46* (43): 8128-8147.
55. Rozas I, Alkorta I, Elguero J. Bifurcated Hydrogen Bonds: Three-Centered Interactions. *J. Phys. Chem. A* **1998;** *102* (48): 9925-9932.
56. Barth, A. The infrared absorption of amino acid side chains. *Prog. Biophys. Mol. Biol.* **2000;** *74* (3-5): 141-173.
57. Barth A. Infrared spectroscopy of proteins. *Biochim. Biophys. Bioenerg.* **2007;** *1767* (9): 1073-1101.
58 Surewicz WK, Mantsch HH, Chapman D. Determination of Protein Secondary Structure by Fourier Transform Infrared Spectroscopy: A Critical Assessment. *Biochemistry* 1993; **32**: 389–394.
59 Valenti LE, Paci MB, De Pauli CP, Giacomelli CE. Infrared Study of Trifluoroacetic Acid Unpurified Synthetic Peptides in Aqueous Solution: Trifluoroacetic Acid Removal and Band Assignment. *Anal. Biochem.* 2011; **410**: 118–123.
60. Ruggeri FS, Longo G, Faggiano S, Lipiec E, Pastore A, Dietler G. Infrared nanospectroscopy characterization of oligomeric and fibrillar aggregates during amyloid formation. *Nat. Commun.* **2015;** *6:* 7831.
61. Henry S, Bercu NB, Bobo C, Cullin C, Molinari M, Lecomte S. Interaction of Aβ1-42 peptide or their variant with model membrane of different composition probed by infrared nanospectroscopy. *Nanoscale* **2018;** *10* (3): 936-940.
62 Silva ER, Listik E, Han SW, Alves WA, Soares BM, Reza M, Ruokolainen J, Hamley IW. Sequence Length Dependence in Arginine/Phenylalanine Oligopeptides: Implications for Self-Assembly and Cytotoxicity. *Biophys. Chem.* **2018**; 233:1-12.

TOC ENTRY